The Braess Paradox and Its Impact on Natural-Gas-Network Performance

Luis F. Ayala H. and **Seth Blumsack,** Pennsylvania State University

Summary

Steady increases in natural gas transportation volumes have prompted operators to reevaluate the performance of the existing gas-pipeline infrastructure. Conventional wisdom dictates that adding an additional link or a pipe leg in a gas-transportation network should enhance its ability to transport gas. Several decades ago, however, Dietrich Braess challenged this traditional understanding for traffic networks. Braess demonstrated that adding extra capacity could actually lead to reduced network efficiency, congestion, and increased travel times for all drivers in the network (the so-called "Braess paradox"). The study of such counterintuitive effects, and the quantification of their impact, becomes a significant priority when a comprehensive optimization of the transportation capacity of operating gas-network infrastructures is undertaken. Corroborating the existence of paradoxical effects in gas networks could lead to a significant shift in how network capacity enhancements are approached, challenging the conventional view that improving network performance is a matter of increasing network capacity. In this study, we examine the occurrence of Braess' Paradox in natural-gas-transportation networks, its impact, and potential consequences. We show that paradoxical effects do exist in natural-gas-transportation networks and derive conditions where it can be expected. We discuss scenarios that can mask the effect and provide analytical developments that may guide the identification of paradoxical effects in larger-scale networks.

Introduction

In the United States, interstate and intrastate gas pipelines are the main source for transporting natural gas from the reservoir to its point of demand. The total pipe mileage of the natural-gas-distribution network in the U.S. is 305,000 miles (US EIA 2008). The steady increase in the production of natural gas during recent years has prompted operators to reevaluate the performance of the existing pipeline infrastructure to accommodate additional new volumes brought into the system. Proper planning of improvements on the existing network on the basis of the forecasted demand for gas is a necessity for pipeline-operating companies. The cost associated with operating and managing such large pipeline systems is directly related to the energy loss; these losses have to be addressed by the process of optimization to keep costs at a minimum. The ultimate goal is for natural-gas-transportation networks to be efficiently designed or modified such that a maximum amount of gas is transported with minimum energy losses.

Generally, adding an additional link or a pipe leg in a gas-transportation network is assumed to ease the gas flow and increase network capacity. In 1968, Dietrich Braess analyzed road-transportation networks and showed that under certain circumstances, the inclusion of a new route in the existing parallel routes may actually create network congestion and increase the total travel time for all users (Braess 1968). This counterintuitive network phenomenon has since been known as the "Braess paradox." **Figs. 1a and 1b** show the network arrangement used by Braess. In Fig. 1, point 1 is the origin of traffic flow and point 4 is the destination for the traffic flow. In Fig. 1a, there are two possible routes (124 and 134) for traffic to flow from origin to destination. Fig. 1b shows the same network, but with a new additional link between points (2,3). This additional link is traditionally referred to as the "Wheatstone bridge" in direct analogy with the classical Wheatstone electrical-circuit configuration presented in **Fig. 2.** In his development, Braess concluded that the addition of the new link (2,3) in Fig. 1b can cause a detrimental reallocation of the existing traffic flow in routes 124 and 134, leading to a bottleneck and an eventual increase in the total travel time for the network users. With this work, Braess challenged the conventional wisdom of traffic planning—that construction of more roads should lead to less congestion and reduced travel times for all users of the network. His analysis showed that links designed to alleviate congestion problems on peripheral routes may cause the opposite effect. This led to a counterintuitive approach to network-performance enhancement: efficiency can actually be improved by removing network links for conditions where the Braess paradox holds.

The Braess paradox did not garner much attention when first identified in the 1960s. Resurgence in interest of the paradox has been sparked by the advent of large-scale "super-networks" (telecommunications, internet, electrical distribution, and energy transportation), exacerbated congestion problems, and increased system complexity. This renewed interest prompted Braess and collaborators to publish the English translation of his original paper for the first time nearly four decades later (Braess et al. 2005), even though the concept of the Braess paradox had been introduced to the English-speaking community by Murchland (1970). Over the past two decades, many investigators have studied the paradox in depth with respect to electrical distribution networks, road transportation networks, mechanical transmission networks, financial networks, and computational sciences (Cohen and Horowitz 1991; Arnott and Small 1994; Korilis et al. 1997; Korilis et al. 1999; Milchtaich 2006; Blumsack 2006; Blumsack et al. 2007; Nagurney et al. 2007; Lin and Lo 2009). Media reports have also indicated that Braess' original insight has been used in several real-world circumstances to improve urban traffic flow by restricting vehicular access to certain areas (Kolata 1990; Wolmar 1994; Fisher 2002; Baker 2009). Increased recognition has indeed given the paradox its own Wikipedia entry since 2004.

Blumsack (2006) and Blumsack et al. (2007) investigated the application of the Braess paradox phenomenon to large-scale electric power networks and found that the paradox indeed occurs in electrical circuits beyond the simple resistor networks described in Cohen and Horowitz (1991). Unlike traffic networks, there is

This paper (SPE 160142) was accepted for presentation at the SPE Annual Technical Conference and Exhibition, San Antonio, Texas, USA, 8–10 October 2012, and revised for publication. Original manuscript received for review 31 July 2012. Paper peer approved 11 October 2012.

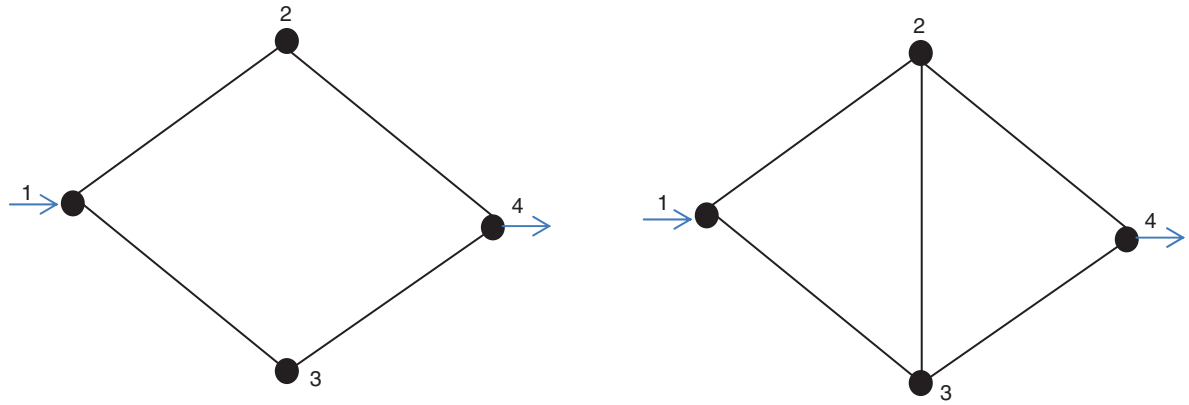

Fig. 1—The Braess network (a) without 2-3 link; (b) with 2-3 link.

no queuing per se in electrical networks, but electrical topology and constraints on transmission links can have a major influence on how power generation assets are used. They showed that the total system cost (defined as the generation cost of serving a fixed amount of system demand) increased when the additional travel route or the Wheatstone bridge (Fig. 2) was added in some locations. The study of the Braess paradox in large-scale electrical networks has suggested not only that network operations may be improved by removing links, but that network upgrade decisions are more complex than simply identifying and expanding the most constrained link.

Calvert and Keady (1993, 1996) presented the first and only studies to date attempting to evaluate the potential manifestation of the Braess paradox in fluid-transportation pipe networks. The authors investigated the paradox in the context of water-supply pipe networks where flow-rate vs. pressure-drop dependence could be described through a Hazen-Williams-type relationship ("power-law nonlinearity"). Their work examined the effects of the paradox in terms of its impact on the value of a power loss (or power consumed) function defined as

$$P = \sum_{(i,j)} \left(p_i - p_j \right) \cdot q_{ij} . \quad \text{.....(1)}$$

The authors argue that the overall cost of fluid-transportation or network pumping requirements can be quantified in terms of changes in this power loss or usage function P. An increased network flow resistance would be associated with increased values of the P-power loss function; therefore, a Braess paradoxical effect would be evident if an increase in the conductivity of a network link could lead to an increase in power usage P. Using a succession of mathematical proofs, their work demonstrated that P is always a decreasing function of pipe conductivities as long as the same type of Hazen-William flow-pressure non-linearity (n in **Table 1**) is used to model flow in all network pipes and the network handles a fixed consumption and supply. Because this is the intuitive, expected behavior for a pipe-network system, Calvert and Keady concluded that the Braess paradox cannot occur in pipe-network systems modeled under such conditions. The authors also show that the Braess paradox may occur in these network systems if different power-law non-linearities (n) were to be used to model flow within different pipes in the same network. While an interesting finding in a mathematical sense, this conclusion had a limited practical implication because fluid network analysis is routinely carried out using the same constitutive equation applied to all network piping components, and therefore uniformly applies the same power-law nonlinearity (n) to all pipes. In our study, we show that even when n is identical for all pipes, Braess paradoxical effects can be observed in natural-gas-transportation networks under some conditions not considered in Calvert and Keady's original studies; derive conditions where the paradox can be observed in natural gas-pipeline networks; and discuss its potential impact on network performance. In our studies, the same flow/pressure drop non-linearity n is used to model flow in all pipes, as is customarily done in network analysis. We implement network equations that are more appropriate for the natural-gas context and honor the additional nonlinearities inherent to gas pipe flow ($s=2$ in Table 1) which are not present in liquid networks (for which $s=1$).

Analysis of Fluid-Transportation Networks

Pipe-network analysis entails the definition of the mathematical model governing the flow of fluids through a transportation and distribution system (Ayala 2013; Larock et al. 2000; Kumar 1987; Osiadacz 1987). Pipeline systems that form an interconnected net or network are composed of two basic elements: nodes and node-connecting elements. Node-connecting elements can include pipe legs, compressor or pumping stations, valves, and pressure and flow regulators, among other components. Nodes are the points where two pipe legs or any other connecting elements intercept or where there is an injection or offtake of fluid.

In pipe-network problems, the analysis consists of determining resulting flow though each pipe and associated nodal pressures. This can be accomplished on the basis of known network topology

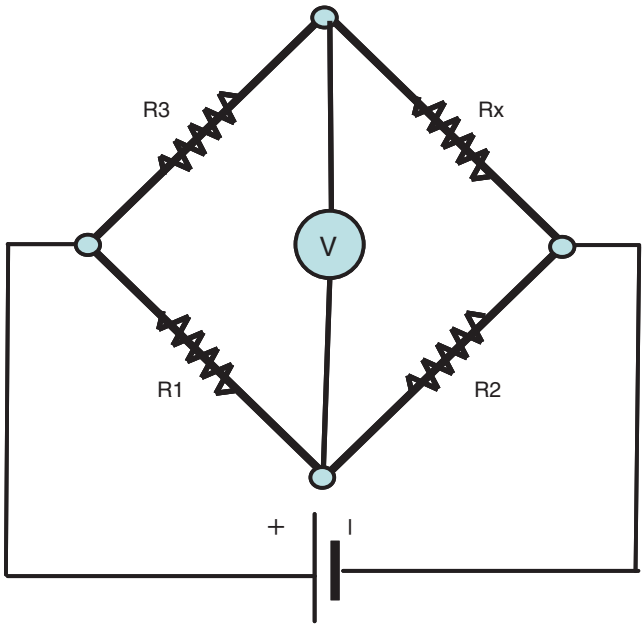

Fig. 2—Classical Wheatstone circuit configuration.

TABLE 1—SUMMARY OF SPECIALIZED EQUATIONS FOR SINGLE-PHASE LIQUID OR GAS FLOW (AYALA 2012)

$$q_{ij} = C_{ij}(p_i^s - p_j^s)^n$$

Liquid Eqs. ($q_{ij} = q_L$)	Friction-Factor Assumption	C_{ij}	m	n	s
Darcy-Weisbach (generalized)	Moody chart or Colebrook Eqn	$\frac{\sigma_L}{\sqrt{\gamma_L f_F}}\frac{d^m}{L^n}$	2.50	0.50	1
Poiseuille's law (laminar flow)	$f_F = \frac{16}{\mathrm{Re}}$	$\frac{\pi \cdot g_c}{128 \cdot \mu_L}\cdot\frac{d^m}{L^n}$	4.00	1	1
Hazen-Williams	$f_F = \frac{K_{HW}}{C_{HW}^{1.852}}\frac{d^{0.13}}{q^{0.148}}$	$\frac{\sigma_{L,HW}^{1.08}\cdot C_{HW}}{\gamma_L^{0.54}}\cdot\frac{d^m}{L^n}$	2.63	0.54	1

where: σ_L,$\sigma_{L\ HW}$ = unit-dependent constants for the conductivity calculation. For q (ft^3/s), L (ft), d (ft), σ_L= 3.15, $\sigma_{L,W}$= 0.4598. For q (ft^3/s), L (ft), d (in.), σ_L= 6.3148·10^{-3}, $\sigma_{L,W}$= 1.08335·10^{-3}. For SI units, σ_L= 1.74, $\sigma_{L,W}$= 0.30614. C_{HW} = Hazen-Williams dimensionless roughness coefficient, C_{HW} =150 for polyvinyl chloride (PVC); C_{HW} =140 for smooth metal pipes and cement-lined ductile iron; C_{HW} =130 for new cast iron, welded steel; C_{HW} =120 for wood and concrete; C_{HW} =110 for clay and new riveted steel; C_{HW} =100 for old cast iron and brick; C_{HW} =80 for badly corroded cast iron. Values above assume the flow of water. Suggested values of C_{HW} for refined petroleum products as a function of temperature are also reported. κ_{HW} = unit-dependent constant in the HW friction empirical equation. κ_{HW}= 46.9334 for d (ft), q (ft^3/s); κ_{HW}= 33.977 for d (in.), q (ft^3/s); κ_{HW}= 32.3045 for SI units.

Gas Eqs. ($q_{ij} = q_{Gsc}$)	Friction-Factor Assumption	C_{ij}	m	n	s
Generalized gas eq.	Moody chart or Colebrook eq.	$\frac{e_f\cdot\sigma_G(\frac{T_{sc}}{p_{sc}})}{\sqrt{SG_G T_{av} Z_{av}}}\cdot\sqrt{\frac{1}{f_F}}\cdot\frac{d^m}{L^n}$	2.50	0.50	2
Weymouth	$f_F = \frac{K_W}{d^{1/3}}$	$\frac{e_f\cdot\sigma_{G,w}(\frac{T_{sc}}{p_{sc}})}{\sqrt{SG_G T_{av} Z_{av}}}\cdot\frac{d^m}{L^n}$	2.666	0.50	2
Panhandle-A (original panhandle)	$f_F = \frac{K_{PA}}{\left(\frac{q_{GSC}\cdot SG_g}{d}\right)^{0.1461}}$	$\frac{e_f\cdot\sigma_{G,PA}(\frac{T_{sc}}{P_{sc}})^{1.078}}{(SG_G^{0.854}T_{av}Z_{av})^n}\cdot\frac{d^m}{L^n}$	2.618	0.54	2
Panhandle-B (modified panhandle)	$f_F = \frac{K_{PB}}{\left(\frac{q_{GSC}\cdot SG_g}{d}\right)^{0.03922}}$	$\frac{e_f\cdot\sigma_{G,PB}(\frac{T_{sc}}{P_{sc}})^{1.02}}{(SG_G^{0.961}T_{av}Z_{av})^n}\cdot\frac{d^m}{L^n}$	2.530	0.51	2
AGA (partially turbulent)	$\frac{1}{\sqrt{f_F}} = 4F_D\log_{10}\left(\frac{\mathrm{Re}\sqrt{f_F}}{1.41}\right)$	$\frac{e_f\cdot\sigma_G(\frac{T_{sc}}{P_{sc}})}{\sqrt{SG_G T_{av} Z_{av}}}\cdot\sqrt{\frac{1}{f_F}}\cdot\frac{d^m}{L^n}$	2.50	0.50	2
AGA (fully turbulent)	$\frac{1}{\sqrt{f_F}} = 4.0\log_{10}\left(\frac{3.7d}{e}\right)$	$\frac{e_f\cdot\sigma_G(\frac{T_{sc}}{P_{sc}})}{\sqrt{SG_G T_{av} Z_{av}}}\cdot\sqrt{\frac{1}{f_F}}\cdot\frac{d^m}{L^n}$	2.50	0.50	2

where: κ_W,κ_{PA},κ_{PB}= unit-dependent constant in the friction empirical equations. κ_W=0.008 for d (in.) or 0.002352 for d (m); κ_{PA} = 0.01923 for d (in.), q (SCF/D) or 0.01954 for d (m), q(sm^3/d); κPB=0.00359 for d (in.), q (SCF/D) or 0.00361 for d (m), q (sm^3/d). σ_G, $\sigma_{G,}$, $\sigma_{G,PA}$, $\sigma_{G,PB}$ = unit-dependent constants for specific resistance calculations. For $qGsc$ (SCF/D), L (ft), d (in.), p (psia), T (R): σ_G= 2,818; $\sigma_{G,}$= 31,508; $\sigma_{G,PA}$=44,400; $\sigma_{G,PB}$=58,328. For $qGsc$ (SCF/D), L (miles), d (in.), p (psia), T (R): σ_G= 38.784; $\sigma_{G,}$= 433.618; $\sigma_{G,PA}$=435.98; $\sigma_{G,PB}$=736.77. For SI units in $qGsc$ (sm^3/d), L (m), d (m), p (KPa), T (K): σ_G= 574,901 ; $\sigma_{G,W}$= 11.854·10^6 ; $\sigma_{G,PA}$=13.656 ·10^6 ; $\sigma_{G,PB}$=13.196·10^6.

and connectivity information, fluid properties, and pipe characteristics combined with mass conservation statements. The analysis assumes knowledge of the constitutive equation for each node connecting elemen (i.e., prior knowledge of the mathematical relationship between flow across the element and its nodal pressures). For the case of single-phase flow of fluids in pipes, these constitutive equations are well-known and are presented in Table 1. Appendix A presents an abridged derivation of these constitutive equation for liquid and gas pipe flow from fundamental principles. In a nodal formulation, fluid-network equations are written on the basis on the principle of mass conservation (continuity) applied to each of the "N" nodes in the system. This yields "N–1" linearly independent equations that can be used to solve for "N–1" unknowns (i.e., nodal pressures) because one nodal pressure is assumed to be specified within the system. In this formulation, nodal mass conservation statements are written in terms of nodal pressures using the pipe flow constitutive equations in Table 1, which yields for horizontal flow:

$$\sum_{ij} C_{ij}\cdot(p_i^s - p_j^s)^n + S - D = 0, \quad \text{..... (2)}$$

where S and D represent external supply or demand (sink/source) present at the node. Eq. 2 is recognized as the first law of Kirchhoff of circuits, in direct analogy to the analysis of flow of electricity in electrical networks, and is the only circuit law needed to solve the system if equations are written in terms of nodal pressures. Once all nodal pressures are known, pipe flows can be determined from the corresponding pipe constitutive equation in Table 1. For the case of gases (s=2), the generalized gas equation (n=0.50) is given as

$$q_{ij} = C_{ij}\cdot\sqrt{p_i^2 - p_j^2}, \quad \text{..... (3)}$$

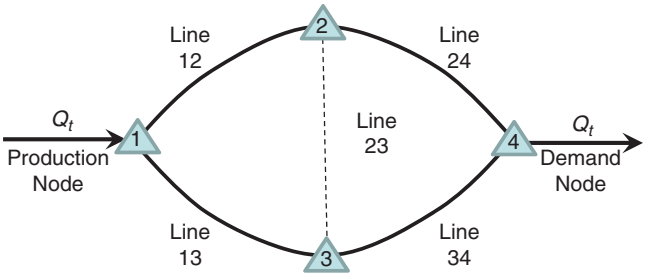

Fig. 3—A Wheatstone structure in a natural-gas transportation network.

where q_{ij}=gas flow through pipe linking nodes i and j (MSCFD), C_{ij}=conductivity of pipe linking nodes i and j (MSCFD/psi), and p_i=pressure at node i. In Table 1, m represents the diameter exponent or power, s is the pressure power that describes the potential nonlinear dependency of fluid density with pressure, and n is the flow exponent ("power-law nonlinearity") of the constitutive pipe equation of choice used for the modeling. The value of n quantifies the type of "power-law non-linearity" used to model pipe flow in the network.

"Finding Braess" in Gas Networks

By drawing analogies with the electric network studies of Blumsack (2006) and Blumsack et al. (2007), this work examines Braess's network arrangement in Fig. 1b in the context of gas networks. This configuration was also explored by Calvert and Keady (1993) for water networks. The Wheatstone network structure of interest, depicted in **Fig. 3** in the context of gas transportation, is the simplest nontrivial network topology where Braess paradoxical effects have been reported in other network systems such as electrical distribution networks, transportation networks, and mechanical transmission networks. [Blumsack (2006) discusses some degenerate cases in two-node networks where Braess paradoxical effects can be observed, although these cases correspond to unrealistic real-life situations.] The structure consists of five pipes and four nodes with a total transportation capacity of Q_t under the total pressure drop (p_1-p_4). All pipes are modeled according to the generalized gas equation in Table 1 (n=0.50, s=2), from where all other gas-pipe equations are derived (Weymouth, Panhandle-A, Panhandle-B, and AGA as discussed in Appendix A). We also choose to work in terms of overall values of pipe conductivities (C_{ij}) that conform to Eq. 3. It is understood that varying a C_{ij}-pipe conductivity value involves changing some characteristics of the fluid or flow properties and/or the pipe geometry (diameter or length) according to the conductivity definitions presented in Table 1.

In this study, we define the existence of Braess's paradoxical behavior as a condition at which a conductivity increase in one of the network pipe links results in either of the following:

- An increased network transportation expense—i.e., an increase in total pressure losses within the structure:

$$\left(\frac{\partial(p_1-p_4)}{\partial C_{link}}\right)>0 \quad \textit{Paradox exists.} \qquad \text{.....(4)}$$

- A decreased total capacity to transport fluids, i.e.,

$$\left(\frac{\partial Q_t}{\partial C_{\text{link}}}\right)<0. \quad \textit{Paradox exists.} \qquad \text{.....(5)}$$

In such paradoxical situation, the removal of such an underperforming pipe link would be beneficial in terms of enhancing the system's ability to transport more fluid or reducing overall transportation costs. For the case of a Wheatstone structure, performance changes are typically monitored with respect to conductivity changes taking place in the redundant line (2,3)—the "Wheatstone bridge"—and the discussion is framed in terms of whether the potential addition or removal of such a bridge would improve or hinder performance.

Unconstrained Wheatstone Structures

Figs. 4 and 5 report pressure and flow rate changes in the Wheatstone configuration in Fig. 3 with respect to changes in the C_{23} conductivity of the Wheatstone pipe bridge when edge-pipe conductivities are $C_{12}=C_{34}=120$ MSCFD/psi and $C_{24}=C_{13}=60$ MSCFD/psi. Total pressure drop across the system (p_1-p_4) is specified to remain constant and equal to 150 psia (Fig. 4). Demand node is maintained at a constant pressure specification of 100 psia (Fig. 4). For this fixed total pressure-drop situation, we study the ability of this network to increase or decrease the total amount of natural gas being transported (Q_t) as the overall network conductivity changes through C_{23}. Simulation is unconstrained [i.e., pipes are assumed to be able to handle increases in pressure and flow without placing any restrictions as the conductivity of the (2,3) bridge changes]. C_{23}-value increases can be accomplished using larger pipe diameters or with additional pipeline looping within the section.

In these figures, the limit $C_{23}\rightarrow 0$ (left side region) represents the situation where the pipe bridge is removed from the network, while

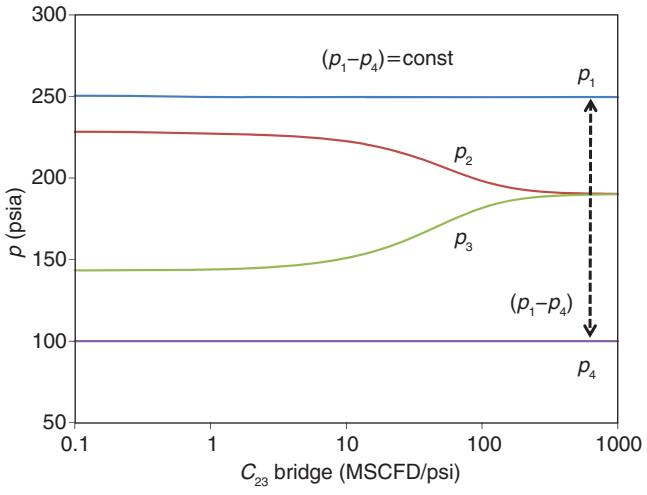

Fig. 4—Network pressure losses vs. bridge conductivity: unconstrained scenario at fixed (p_1-p_4).

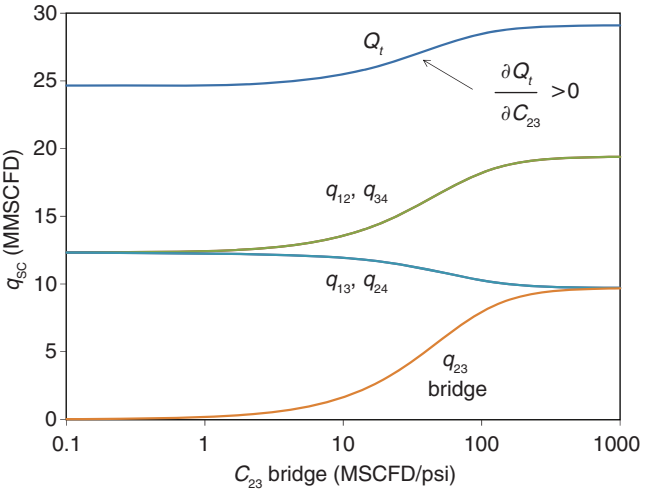

Fig. 5—Pipe transportation capacity vs. bridge conductivity: unconstrained scenario at fixed (p_1-p_4).

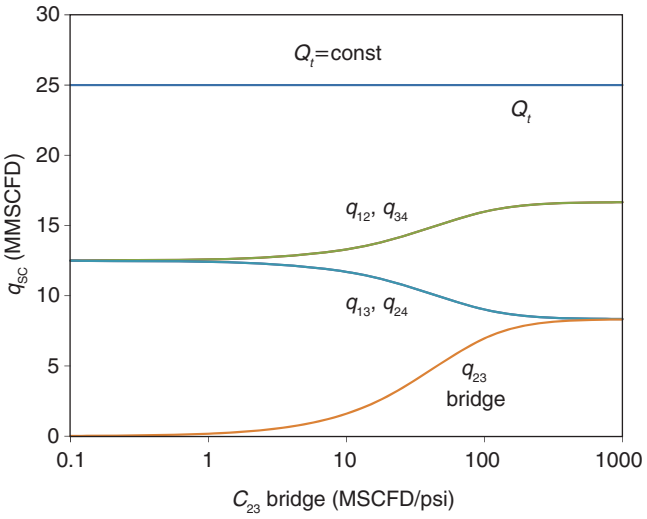

Fig. 6—Pipe transportation capacity vs. bridge conductivity: unconstrained scenario at fixed Q_t.

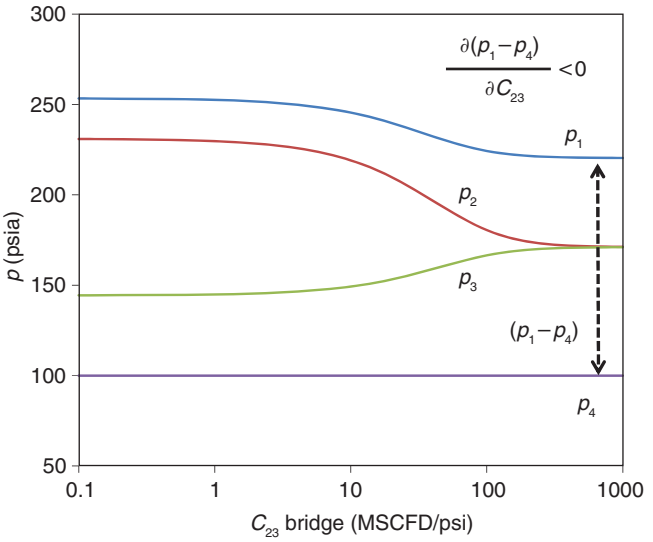

Fig. 7—Network pressure losses vs. bridge conductivity: unconstrained scenario at fixed Q_t.

$C_{23}\rightarrow\infty$ (right side region) represents the limiting situation where nodal pressures p_2 and p_3 converge toward each other because of the infinitely conductive path. Barring any paradoxical effects, one would expect the total transportation capacity of the system (Q_t) to increase when the system is made more conductive. Fig. 5 indeed shows that

$$\left(\frac{\partial Q_t}{\partial C_{23}}\right)>0 \quad \textit{Paradox does not occur} \quad \text{.....(6)}$$

for all values of C_{23} (bridge conductivity) (i.e., an increase in bridge conductivity leads to an increase in transportation capacity for the entire network). **Figs. 6 and 7** alternatively examine the case where total desired transportation capacity is held constant (Q_t=25 MMSCFD), and one examines the variable cost (p_1-p_4) that might be associated with the operation when C_{23} changes. Pipe conductivities remain at $C_{12}=C_{34}=120$ MSCFD/psi and $C_{24}=C_{13}=60$ MSCFD/psi and demand node is maintained at 100 psia. Simulation remains unconstrained, with no restrictions placed on the ability of any of the pipes to handle the associated volumes and pressures as system conductivity increases. Fig. 7 shows, again, that for the proposed scenario,

$$\frac{\partial(p_1-p_4)}{\partial C_{23}}<0 \quad \textit{Paradox does not occur} \quad \text{.....(7)}$$

where it is clear that it becomes progressively easier, and thus less expensive, to transport the specified Q_t=25 MMSCFD fluid volume through this system if network conductivity is increased by C_{23}.

In order to generalize these observations for any gas Wheatstone system, as to rule out the possibility of the existence of any other permutation of C_{12}, C_{34}, C_{24}, C_{13}, Q_t, p_4 that might change the direction of the inequalities stated in Eqs. 6 and 7, we seek an analytical expression for these derivatives. The difficulty in doing so lies within the significant nonlinear nature of the resulting equations and the presence of the nonlinear flow (n) and pressure (s) powers involved in gas analysis. In order to overcome this, we invoke the linear-pressure analog transformation proposed by Ayala (2013). The method consists in defining an alternate, analog system of pipes that obey a much simpler pipe constitutive equation (i.e., a linear-pressure analog flow equation), which is written for horizontal flow as follows:

$$q_{ij}=L_{ij}\cdot(p_i-p_j), \quad \text{.....(8)}$$

where L_{ij} is the value of the *linear pressure analog* conductivity. Note that Eq. 8 uses the flow-pressure drop dependency prescribed by the Hagen-Poiseuille's law (n=1) for liquid flow (s=1) listed in Table 1. Consequently, the proposed analog seeks to map the highly nonlinear gas-flow network problem into a much more tractable liquid analog model for laminar flow conditions. When gas-pipe flows are recast in terms of such linear pressure analog, nodal mass balances used in nodal formulations (Eq. 2) collapse to a much simpler (and more importantly, linear) set of algebraic equations shown here:

$$\sum L_{ij}\cdot(p_i-p_j)+S-D=0, \quad \text{.....(9)}$$

which can be simultaneously solved for all nodal pressures in the network using any standard method of solution of linear algebraic equations, as opposed to its nonlinear counterpart of Eq. 3. Ayala (2013) shows that linear-pressure analog conductivities are straightforwardly calculated as a function of actual pipe conductivities (C_{ij}) according to the following transformation rule:

$$L_{ij}=T_{ij}\cdot C_{ij}, \quad \text{.....(10a)}$$

where T_{ij} is the analog-pipe conductivity transform which is uniquely defined as a function of the pipe pressure ratio ($r_{ij}=p_i/p_j$, where i corresponds to the upstream node) as shown:

$$T_{ij}=\sqrt{1+\frac{2}{r_{ij}-1}} \quad \text{.....(10b)}$$

from where it follows that $T_{ij}>1$ always ($L_{ij}>C_{ij}$).

Appendix B shows that for the unconstrained analysis of the Wheatstone structure in Fig. 3 in terms of its linear analog, the Braess paradox can happen only if

$$(L_{12}L_{34}-L_{24}L_{13})^2<0, \quad \text{.....(11a)}$$

which in terms of actual conductivities and for the actual system yields the condition

$$(T_{12}T_{34}\cdot C_{12}C_{34}-T_{24}T_{13}\cdot C_{24}C_{13})^2<0, \quad \text{.....(11b)}$$

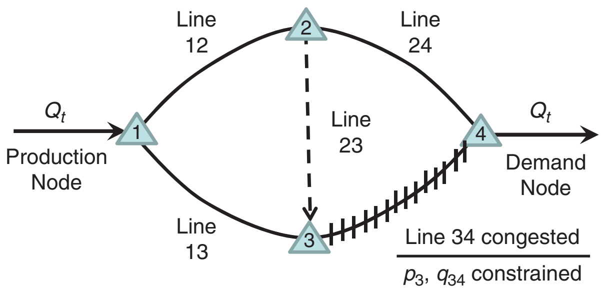

Fig. 8—A natural gas Wheatstone structure with a congested pipe (line 34).

which can be never true regardless of C_{ij} and T_{ij} values. Please note that this is an inequality that is independent of values of bridge conductivity, Q_t, and p_4 specifications.

Therefore, it is concluded that the Braess' paradox *will never occur* in unconstrained two-terminal (one supply node, one demand node) Wheatstone gas-transportation structures [Blumsack (2006) discusses ways to generate Braess' paradox in two-terminal networks with quantity transfer constraints along specific network branches]. This is actually consistent with the trends depicted in Figs. 4 through 7, which we now recognize are general trends, and corroborates the findings of Calvert and Keady (1993) for water networks. Calvert and Keady's work had stated that unconstrained fluid networks for which pipes are modeled with the same type of power-law nonlinearity (n), much as we have considered throughout our study, should not exhibit Braess's paradoxical behavior.

Constrained Wheatstone Structures

A key assumption in our previous examples was to accept that all pipes were physically able to handle any amount of flow and pressure regardless of the operational changes imposed on the system ("unconstrained" modeling). In reality, there are physical limits to pipeline mechanical strength and to pipe capacity. If we were to acknowledge pipe's physical capacity limits in terms of maximum allowable pressure (MAOP) ratings and associated maximum pipe capacity (q_{max}), a different picture can emerge. In doing so, we now model the system under "congested" (constrained) conditions as illustrated in **Fig. 8.**

Unconstrained modeling the Wheatstone structure in Fig. 3 demonstrated that adding the Wheatstone bridge at (2,3) rerouted parts of the flow from node 2 towards node 3, with the net effect of increasing the pressure at node 3 (p_3) and consequently increasing the flow handled by pipe (3,4) (see Figs. 4 through 7). This model assumed that pipe (3,4) had the strength necessary to handle the increased mechanical stress. Let us now assume that the maximum allowable pressure for safe operation of pipe (3,4) is reached by node 3 at some point during the pressure ramp-up depicted in Figs. 4 and 7. **Figs. 9 and 10** show the associated network performance when the maximum allowable pressure at node 3 is placed at, say, 160 psia. Again, $C_{12}=C_{34}=120$ MSCFD/psi, $C_{24}=C_{13}=60$ MSCFD/psi, $p_4=100$ psia (specified). Please note that by constraining node 3 not to reach pressures beyond 160 psia, the maximum capacity of pipe (3,4) is constrained to $q_{max}=15$ MMSCFD.

Fig. 9 shows that the network ability to transport (Q_t) can be significantly hindered when pipe (3,4) is congested, despite the fact that the network conductivity is increasing. In Fig. 9, once pipe (3,4) gets congested, further increases in bridge conductivity only make matters worse. Interestingly, the elimination of the bridge would eliminate the congestion at (3,4) and restore the ability of the network to transport 25 MMSCFD of gas.

It is also possible to reverse the observed response of total network transportation capacity (Q_t) to changes in C_{23} by manipulating conductivity values for the noncongested pipe edges. **Figs. 11 and 12** show, for example, updated network performance snapshots when uncongested pipe edges have conductivities of $C_{12}=60$ MSCFD/psi and $C_{24}=C_{13}=120$ MSCFD/psi and the conductivity and pressure rating constraints of the congested pipe are maintained ($C_{34}=120$ MSCFD/psi, $p_{max}=160$ psia). While it is apparent in Fig. 11 that the original Q_t-paradoxical effect of Eq. 12a has been successfully reversed [$\partial Q_t/\partial C_{23}>0$], it is interesting to note that the situation remains paradoxical because Fig. 12 now shows that

$$\left(\frac{\partial(p_1-p_4)}{\partial C_{23}}\right) > 0 \quad \textit{Paradox occurs} \quad \text{(12b)}$$

i.e., in both situations, congestion has led to the appearance of the paradox within the network system.

It should be noted that the sign reversal in $\partial Q_t/\partial C_{23}$ is directly linked to the *flow-direction reversal* in the bridge pipe (2,3). This is evident from $q_{23}<0$ in Fig. 11 and $p_3>p_2$ in Fig. 12. In other words, network properties were manipulated in a way such that the direction of flow in the bridge pipe was reversed and the situation forced a fluid rerouting within the network that affected $\partial Q_t/\partial C_{23}$. It is

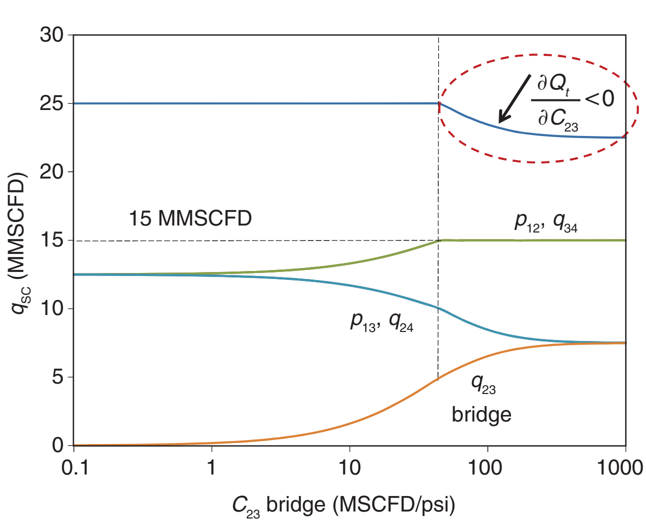

Fig. 9—Pipe transportation capacity vs. bridge conductivity: constrained scenario (I).

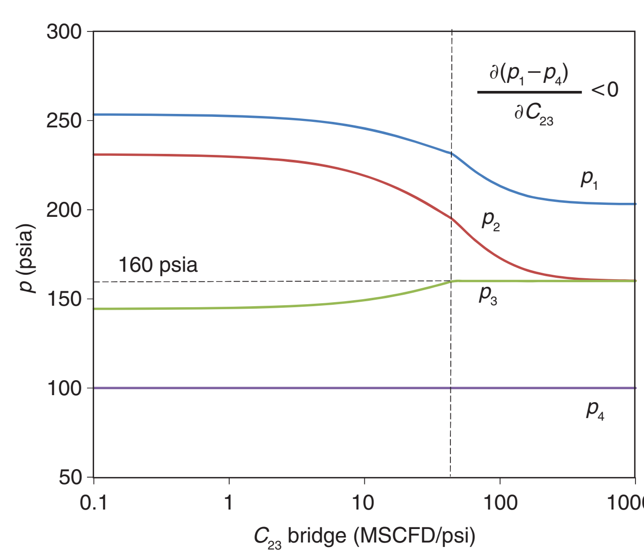

Fig. 10—Network pressure losses vs. bridge conductivity: constrained scenario (I).

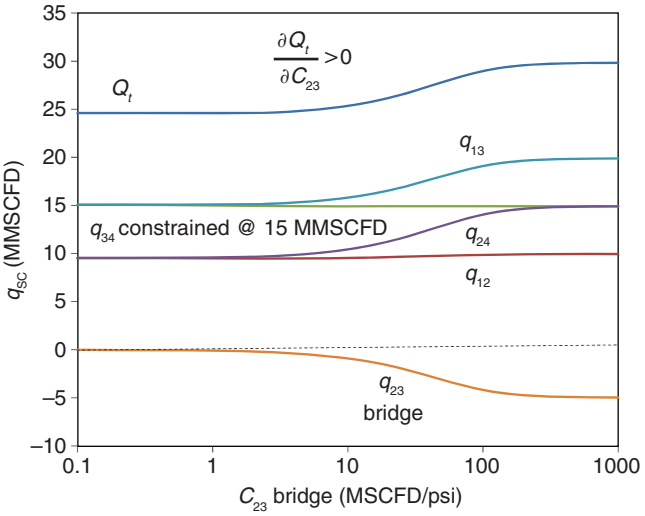

Fig. 11—Pipe transportation capacity vs. bridge conductivity: constrained scenario (II).

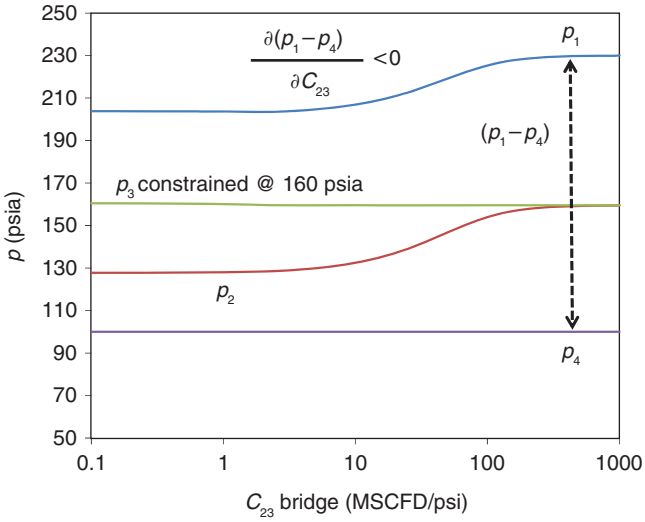

Fig. 12—Network pressure losses vs. bridge conductivity: constrained scenario (II).

straightforward to demonstrate, using the same linear analog technique described in Appendix B, that the condition that controls the sign of $\partial Q_t/\partial C_{23}$ in this congested Wheatstone structure is given by

$$\text{sign}\left(\partial Q_t / \partial C_{23}\right) = -\text{sign}(L_{12}L_{34} - L_{24}L_{13}), \quad \text{..... (13a)}$$

where the condition

$$L_{12}L_{34} - L_{24}L_{13} = 0 \quad \text{..... (13b)}$$

is the zero-flow condition at bridge (2,3) that controls the sign change. In terms of actual pipe conductivities, this condition is rewritten as

$$T_{12}T_{34} \cdot C_{12}C_{34} - T_{24}T_{13} \cdot C_{24}C_{13} = 0. \quad \text{..... (13c)}$$

However, because $q_{23}=0$ implies $p_2=p_3$, the pipe pressure ratios are such that $r_{12}=r_{13}$ and $r_{24}=r_{34}$ at this condition. This means that $T_{12}=T_{13}$, $T_{24}=T_{34}$, and then $T_{12}T_{34}=T_{24}T_{13}$. Therefore, the sign reversal condition becomes

$$C_{12}C_{34} - C_{24}C_{13} = 0 \quad \text{..... (13d)}$$

for the nonlinear Wheatstone gas system. Therefore,

$$C_{12}C_{34} > C_{24}C_{13} \text{ leads to } \left(\partial Q_t / \partial C_{23}\right) < 0 \quad \text{..... (13e)}$$

$$C_{24}C_{13} > C_{12}C_{34} \text{ leads to } \left(\partial Q_t / \partial C_{23}\right) > 0 \quad \text{..... (13f)}$$

Please note that condition (13e) is satisfied by the conductivities used in Figs. 9 and 10, while the condition expressed by Eq.13f is satisfied by the conductivities used to generate Figs. 11 and 12.

Embedded Wheatstone Structures

Even when one overlooks the effects that pipe congestion can have on transmission networks, we have found that Braess paradoxical behavior is possible when uncongested Wheatstone structures are found embedded within a larger network. This situation is depicted in **Fig. 13.** Q_t is the total transportation capacity of the substructure, $k \cdot Q_t$ is the amount of fluid leaving the substructure at node 2, and $(1-k) \cdot Q_t$ is the amount leaving at node 4. In this depiction, k is the fluid takeoff ratio ($0<k<1$) prescribed by downstream conditions found in the larger network. Please note that the condition $k=0$ collapses this formulation to the same unconstrained Wheatstone models presented earlier for which no paradox exists. It can be demonstrated that varying demand requirements imposed on the Wheatstone structure by the larger network (i.e., a varying value of k) can play a pivotal role in the manifestation of the Braess paradox within the substructure.

Figs. 14 and 15 revisit the unconstrained Wheatstone scenario (assuming fixed Q_t) of Figs. 6 and 7, where all network properties are identical ($C_{12}=C_{34}=120$ MSCFD/psi, $C_{24}=C_{13}=60$ MSCFD/psi, $Q_t=25$ MMSCFD, $p_4=100$ psia) except that fluids can now leave through nodes 2 and 4 ($k\neq 0$). In this scenario, 9 MMSCFD are leaving through node 2 ($k=0.36$) and 16 MMSCFD through node 4 ($1-k=0.64$). Simulation is unconstrained (i.e., pipes are assumed to be able to handle increases in pressure without restrictions as bridge conductivity changes). It is noted that Figs. 14 and 15 ($k=0.36$) essentially mimic the network performance trends of Figs. 6 and 7 ($k=0$) where no evidence of paradoxical behavior was found. This, however, is largely dependent on the value of the fluid take-off split k demanded of the Wheatstone substructure by the larger network. We have established that there may exist a fluid take-off split condition (k) able to trigger the appearance of the paradox. **Figs. 16 and 17** reexamine the same scenario when more

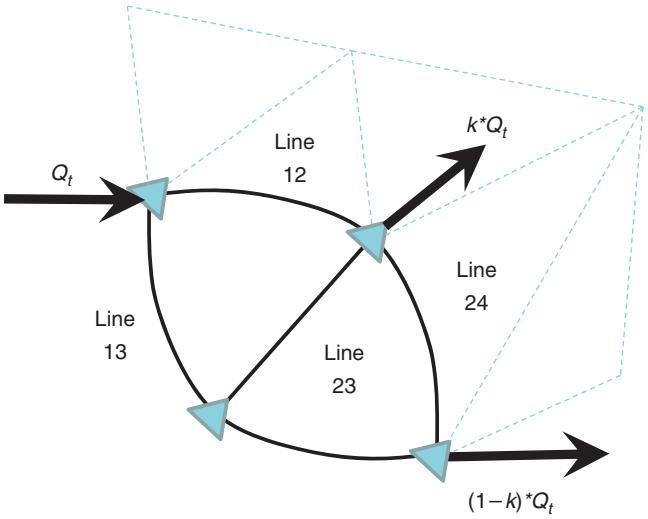

Fig. 13—Embedded Wheatstone structure within a larger natural-gas network.

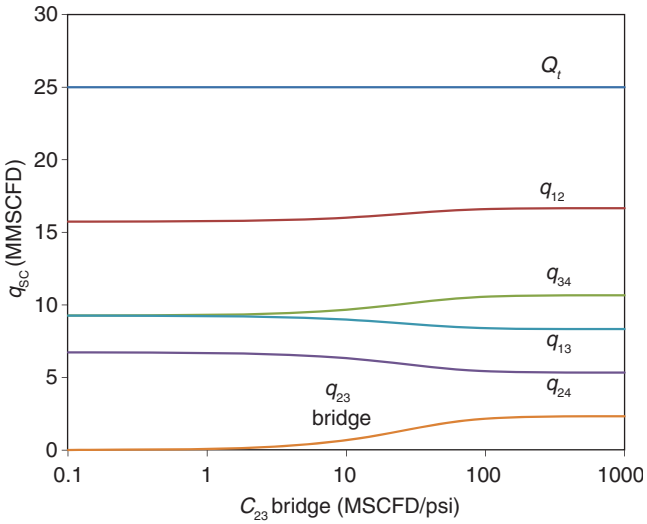

Fig. 14—Pipe transportation capacity vs. bridge conductivity: embedded Wheatstone (k=0.36).

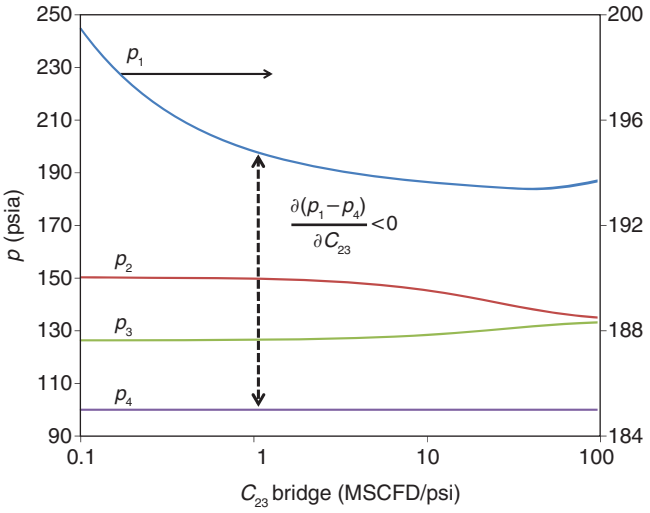

Fig. 15—Network pressure losses vs. bridge conductivity: embedded Wheatstone (k=0.36).

gas (15 MMSCFD) is being demanded at node 2 (k=0.60). Fig. 17 shows that such a demand increase has triggered the paradoxical condition, in which inlet-pressure requirements can only increase if network conductivity is increased. In such situation, the counter-intuitive action of removing the pipe link (2,3) would actually improve the performance of the substructure.

Close examination of Figs. 14 through 17 reveals that appearance of paradoxical effects is directly linked to the occurrence of flow reversals at the (2,3) Wheatstone bridge. Such events can be analytically predicted. By invoking the linear analog method, it can be demonstrated that there exists a critical value of k (k_c) that controls the flow reversal at the bridge and thus the sign of $\partial(p_1-p_4)/\partial C_{23}$. Appendix C shows that such critical value is predicted by the expression

$$k_c = \frac{L_{12}L_{34} - L_{24}L_{13}}{L_{34}(L_{12}+L_{13})} = \frac{T_{12}T_{34}\cdot C_{12}C_{34} - T_{24}T_{13}C_{24}C_{13}}{T_{34}C_{34}(T_{12}C_{12}+T_{13}C_{13})}, \quad \text{..... (14)}$$

where $\partial(p_1-p_4)/\partial L_{23}>0$ (paradoxical condition) for $k>k_c$ and $\partial(p_1-p_4)/\partial L_{23}<0$ for $k<k_c$.

The tipping point for the flow reversal condition ($k=k_c$) in Eq. 14 represents the no-flow situation at the bridge pipe. We have shown that, for such condition, $T_{12}=T_{13}$, $T_{24}=T_{34}$ and $T_{12}T_{34}=T_{24}T_{13}$ for the linear analog. This allows Eq. 14 to collapse to

$$k_c = \frac{C_{12}C_{34} - C_{24}C_{13}}{C_{34}(C_{12}+C_{13})}, \quad \text{..... (15)}$$

which predicts this flow reversal for the nonlinear, embedded Wheatstone structure. It is important to highlight that Eq. 15 is fully able to predict bridge-flow reversal conditions for nonlinear networks. It predicts k_c=0.50 for the Wheatstone networks considered in this section. This explains why k=0.36 in Figs. 14 and 15 (and k=0, for that matter, earlier in the manuscript) did not lead to paradoxical behavior. However, k=0.60 indeed led to paradoxical behavior (Figs. 16 and 17) because the critical tipping point was found at k_c=0.50. This concept is further illustrated in **Fig. 18,** where it is shown that all values of $k>k_c$=0.50 force flow reversals in the bridge ($q_{23}<0$) for the stated conductivities. **Fig. 19** demon-

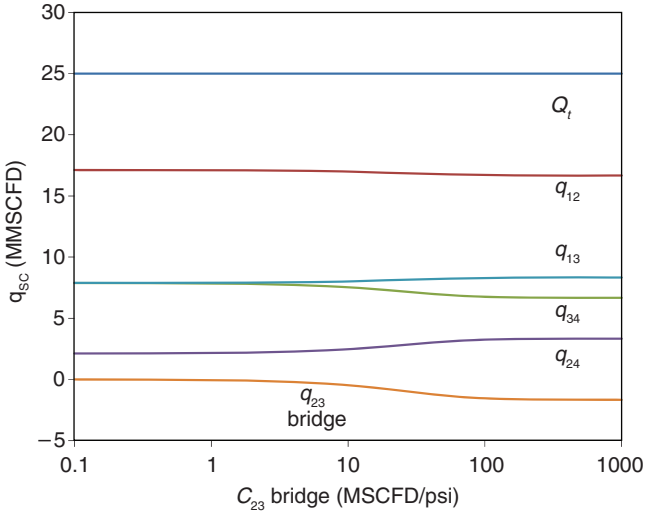

Fig. 16—Pipe transportation capacity vs. bridge conductivity: embedded Wheatstone (k=0.60).

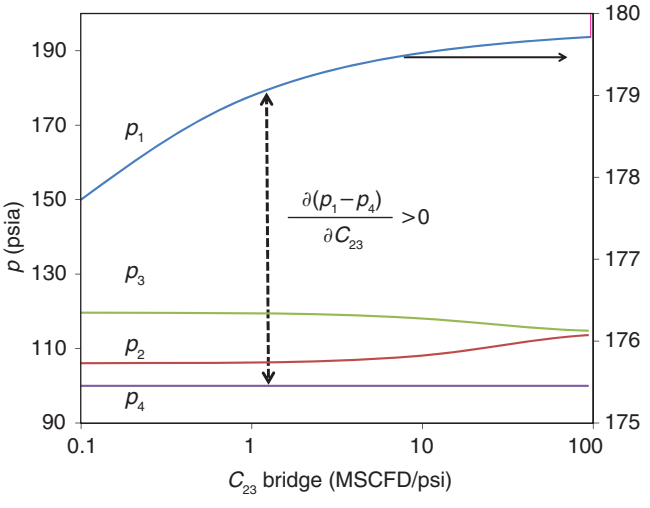

Fig. 17—Network pressure losses vs. bridge conductivity: embedded Wheatstone (k=0.60).

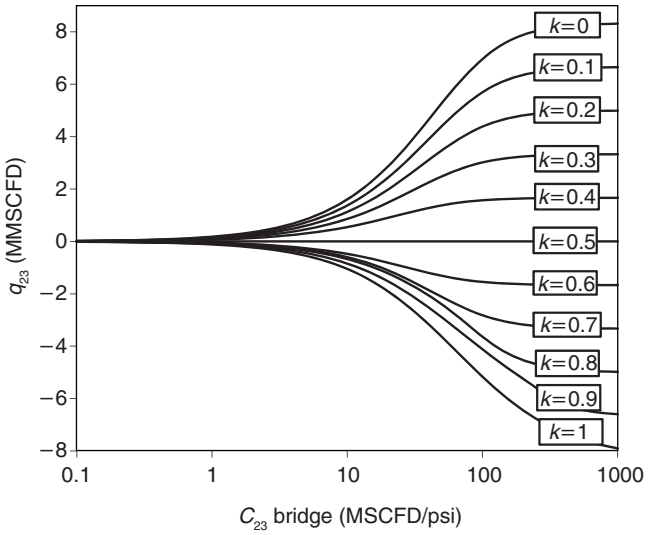

Fig. 18—Bridge flow rate (q_{23}) vs. fluid takeoff ratio (k) and bridge conductivity (C_{23}).

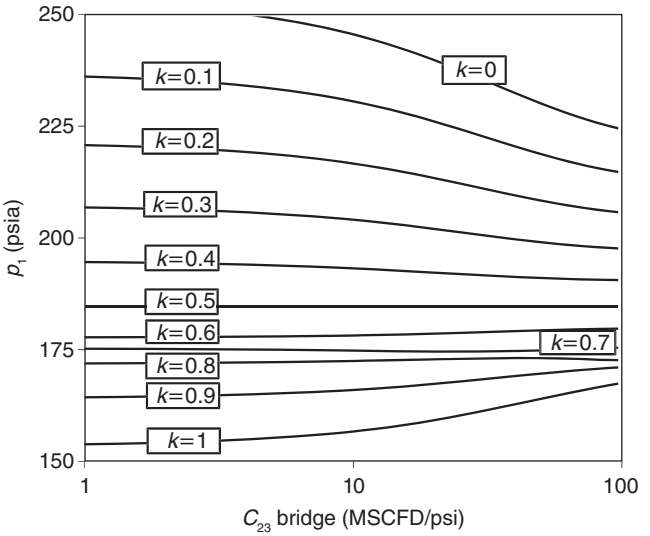

Fig. 19—Required network inlet pressure (p_1) vs. fluid takeoff ratio (k) and bridge conductivity (C_{23}).

strates that such flow reversals at $k>0.50$ come associated with the condition $\partial p_1/\partial C_{23}$ which describes the paradoxical behavior. It is also important to point out that while Eq. 15 can rigorously predict the no-bridge-flow condition at $k=k_c$, the residual presence of the pressure-dependent coefficients T_{12}, T_{34}, T_{24}, T_{13} in Eq. 14 for $k\neq k_c$ can make $\partial p_1/\partial C_{23}$ take values other than negative (for $k<k_c$) or positive (for $k>k_c$) for all possible combinations of C_{23} in the nonlinear case.

Eq. 15 establishes that unconstrained Wheatstone networks with $C_{12}C_{34}>C_{24}C_{13}$ will always have associated a positive value of $k_c>0$ at which paradoxical behavior may become possible. This rules out paradoxical behavior for such networks when $k=0$ ($<k_c$), which further corroborates our earlier findings in unconstrained two-terminal networks (one source and one sink). **Fig. 20** displays the sensitivity of critical fluid takeoff ratio with respect to changes in edge-pipe conductivities for the case $C_{12}=C_{34}=120$, $C_{24}=C_{13}=60$ MSCFD/psi, which has $k_c=0.50$ as its base case. Along any line in Fig. 20, the rest of the conductivities remain at its original values while only one of them changes. It becomes clear from this figure that careful manipulation of edge conductivity values can recreate conditions at which the paradox can be avoided or induced for different conditions of fluid takeoff at node 2.

We finalize our discussion with an important observation about the selection of the mathematical criteria used to identify or rule out the presence of Braess paradoxical behavior in fluid networks. As discussed throughout our manuscript, we have used the detection criteria stated in Eqs. 4 and 5. Calvert and Keady (1993), however, used the concept of power loss or usage function given in Eq. 1, and defined the paradox as a situation that caused network power consumption P to increase when conductivity increases (i.e., $\partial P/\partial C_{23}>0$). The authors also constrained their definition to cases where transportation capacity Q_t was held constant. **Fig. 21** shows the results of applying the power-loss function definition in Eq. 1

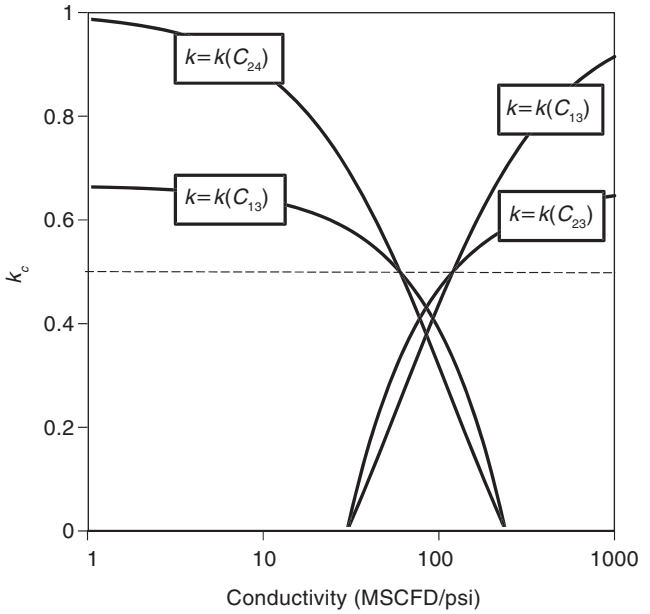

Fig. 20—Critical fluid-takeoff ratio dependency on edge-pipe conductivities.

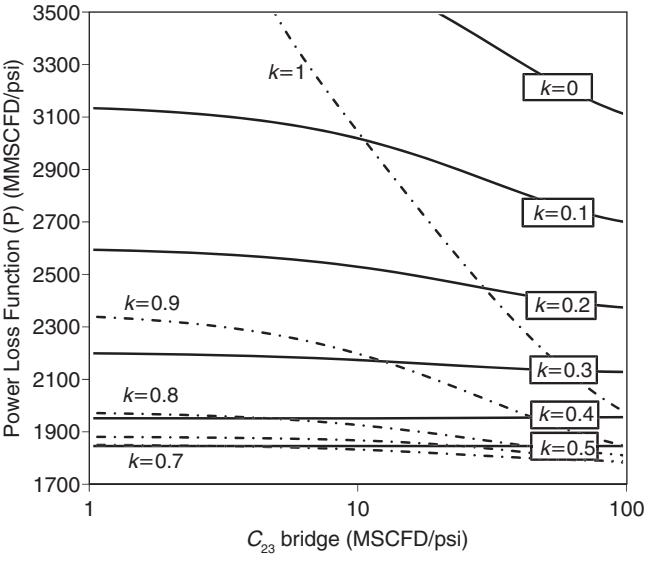

Fig. 21—Calvert and Keady's power-loss function for the embedded Wheatstone structure.

to all cases shown in Fig. 19. In all these cases, transportation capacity Q_t is being held constant. Notably, it is evident that Figs. 19 and 21 convey very different and contradictory messages of paradox detection. According to Fig. 21 and Calvert and Keady's criteria, no paradoxical behavior is present in any of the embedded Wheatstone scenarios presented in Fig. 19 given that $\partial P/\partial C_{23}<0$ for all *k*s. This is actually consistent with Calvert and Keady's development, which had ruled out the possibility of paradoxical behavior in unconstrained three-terminal Wheatstone structures (and any other fluid network structure for that matter) that used the same power-law non-linearity (n) to model fluid flow in all pipes, as has been done in this study. Fig. 19 clearly shows, however, that paradoxical behavior is present at all *k*s>0.50. Transportation costs in gas networks are directly linked to the fuel consumption of compressors driving the process. An operator handling a compressor at node 1, in charge of delivering the required system's inlet pressure p_1, would observe that the system's power (fuel) consumption would only increase when conductivity increases, given that the required compressor discharge (p_1) keeps moving up along with conductivity for *k*s>0.50 (Fig. 19). For this case, the power loss function in Eq. 1 fails to capture such a power (fuel) consumption increase. This seems to suggest that Eq. 1 is able to diagnose false negatives when used as a screen to predict Braess paradoxical behavior. The imprecision of the power-loss function is further illustrated in **Fig. 22,** which examines the behavior of the power-loss function for all other cases considered in our study. The curve in Fig. 22 labeled "Figs. 6 and 7" assumes a constant level of gas demand Q_t; in this case, the power-loss equation correctly predicts that the Braess paradox will not occur. For all other cases in Fig. 22, use of the power-loss screen yields a false result—either the power-loss equation predicts paradoxical behavior when in fact none is exhibited. or the power-loss equation fails to correctly predict the presence of paradoxical behavior. These findings leave the door open for potential detection of paradoxical behavior in fluid networks that had originally been ruled out by Calvert and Keady's study as unable to exhibit the Braess paradox.

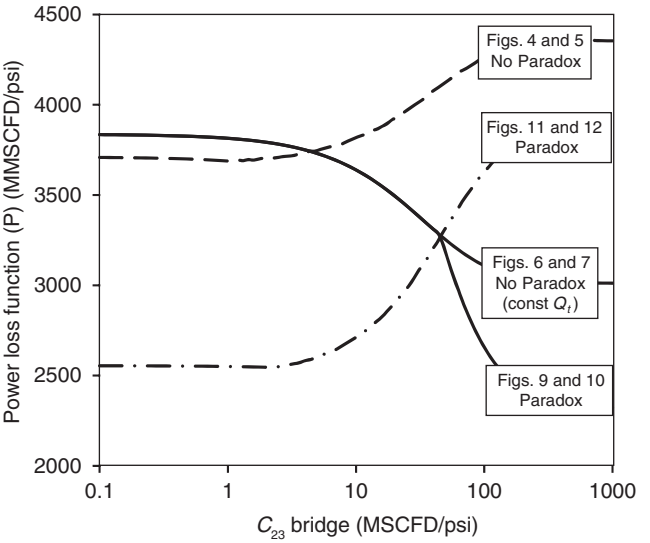

Fig. 22—Calvert and Keady's power-loss function for constrained and unconstrained two-terminal Wheatstone cases.

Conclusions

Managing natural gas infrastructure networks in the face of increasing supplies and potentially shifting sectoral demands is a complex challenge. The traditional response to scarcity in network infrastructure has been to increase network capacity, either overall or in certain targeted areas. While we do not question the need for new infrastructure in many situations, we question the conventional wisdom that building more is always better. In particular, our analytical experiments with simple natural-gas networks suggest that industry should pursue a dual strategy of upgrading severe bottlenecks while simultaneously examining existing assets with a fresh perspective toward improved use. In particular, we suggest that a process of identifying and removing underperforming pipe links would, in some cases, be a lower-cost alternative to achieve a given measure of improved network performance. We also find that in some cases, changes in network topology or/and demand conditions can lead to reversal of fluid flow. Flow reversals can cause paradoxical behavior to appear in networks and cause them to disappear when they already exist [negation of the paradox caused by flow reversals triggered by increased network demands is a conclusion that is similar to that of Nagurney (2010) for traffic networks]. This finding suggests that decisions on the operational time frame may, in some cases, be sufficient to negate or reverse the paradox.

Flow reversals that can negate or support Braess's paradoxical behavior are only possible in networks with built-in backup or redundant routes. This is the case for many large, complex networks where reliable and continuous delivery of a commodity is a priority and the likelihood of any delivery disruption is minimized by creating multiple (redundant) delivery paths. Because Braess's paradoxical behavior is inextricably linked to the possibility of flow reversals within the structure, single pipes, pipes in parallel [with some special exceptions as Blumsack (2006) has discussed], pipes in series, and any branching, loopless networks may not exhibit Braess paradoxical behavior. In these simpler, loopless structures, changes in network conductivity or supply/demand conditions essentially rescale pipe-flow *magnitudes*, but do not alter any of the pipe-flow *direction*s, thus negating the possibility of paradoxical behavior. It was shown, however, that not all flow reversals are necessarily detrimental to network performance, as was clearly the case for unconstrained two-terminal Wheatstone structures.

The analytical experiments presented in this paper demonstrate that the Braess paradox can manifest itself in natural gas networks, where the "user cost" is defined in terms of commodity deliverability or pressure requirements. Our analysis essentially confirms some conclusions of Calvert and Keady (1993), but reevaluates and extends their findings by using network equations that are more appropriate for the natural-gas context. We also highlight potential inconsistencies in Calvert and Keady's method for evaluating the paradox in fluid networks, finding that the use of their screening function (the power-loss equation) can lead to false-negative or false-positive diagnoses of paradoxical behavior. While much of the attention of this paper has been on the Wheatstone network structure [drawing analogies with Blumsack (2006) and Blumsack et al. (2007)], we emphasize that identifying paradoxical topologies in natural-gas networks is more complex than simply identifying all possible Wheatstone subnetworks. In particular, when natural-gas networks are constrained in some way, it is possible to see the paradox in a series-parallel topology with built-in redundancies [Blumsack (2006) also found this for electrical networks]. The process of "finding Braess" in large networks entails the identification of all backup routes or network redundancies prone to flow reversals and evaluation of their overall effect on network performance. Phillips (2012) has explored this avenue for natural-gas networks with as many as 100 pipes and has presented a methodology for testing such networks that decomposes them into smaller equivalent substructures. She has also applied an economic model that evaluates the best options available to a network operator for cases where the paradox has been detected in the network.

Nomenclature

A = pipe cross-sectional area, L^2
B = number of pipe branches in a pipe network

C_{HW} = Hazen-Williams dimensionless roughness coefficient
C_{ij} = pipe conductivity of pipe (i,j) used in generalized gas flow equation, $L^4\ m^{-1}\ t$
d = pipe internal diameter, L
D = fluid demand at a node in a pipe network, $L^3\ t^{-1}$
e = pipe roughness, L
e_f = pipe flow efficiency factor
f_F = Fanning friction factor
FD = AGA drag factors
g = acceleration of gravity, $L\ t^{-2}$
g_c = mass/force unit conversion constant, $m\ L\ F^{-1}\ t^{-2}$ (32.174 lbm ft $lbf^{-1}\ s^{-2}$ in Imperial units; 1 Kg m $N^{-1}\ s^{-2}$ in SI)
h = elevation with respect to datum, L
k = fluid takeoff ratio for the embedded Wheatstone structure
L = pipe length, L
L_{ij} = linear-analog pipe conductivity, $L^4\ m^{-1}\ t$
m = diameter power or exponent
MW = molecular weight, m/n
n = flow power (exponent) or power-law non-linearity
N = number of nodes in a pipe network
p = pressure, $m\ L^{-1}\ t^{-2}$
P = power-loss function in Eq. 1
q_{ij} = gas flow rate at standard conditions for pipe (i,j), $L^3\ t^{-1}$
Q_t = total transportation capacity of pipe network, $L^3\ t^{-1}$
r_{ij} = pressure ratio for the linear-pressure analog method
R = universal gas constant, $m\ L^2\ T^{-1}\ t^{-2}\ n^{-1}$ (10.7315 psia-ft^3 $lbmol^{-1}\ R^{-1}$ in English units or 8.314 m^3 Pa K^{-1} $gmol^{-1}$)
s = pressure power in pipe-flow equation
S = network supply at a given node
SG_G = gas specific gravity
T = absolute temperature
T_{ij} = analog conductivity transform
v = fluid velocity, $L\ t^{-1}$
W = mass flow rate, $m\ t^{-1}$
x = pipe axial axis, L
z = pipe elevation axis; or axial component, L
Z = fluid compressibility factor
α = rate-dependent integration term in the energy balance, $m^2\ L^{-5}\ t^{-2}$
β = elevation-dependent integration term in the energy balance, $L\ t^{-2}$
γ_L = liquid specific weight, $m\ L^{-2}\ t^{-2}$
η = gas density dependency on pressure
$\kappa_W,\kappa_{PA},\kappa_{PB}$ = unit-dependent constants for the gas friction factor equations
μ = fluid dynamic viscosity, $m\ L^{-1}\ t^{-1}$
π = ratio of the circumference of a circle to its diameter=3.14159265…
ρ = fluid density, $m\ L^{-3}$
σ_G = unit-dependent constant for the gas-flow equation, $T\ t^2\ L^{-2}$
σ_L = unit-dependent constant for the liquid flow equation, $L\ t^{-2}$
ϕ = gas density dependency on pressure, $t^2\ L^{-2}$
Ω_G = conductivity coefficients in the linear-analog network formulation (Appendices B and C)

Subscripts

av = average
f = friction
G = gas
i = pipe entrance
j = pipe exit
L = liquid
sc = standard conditions (60 F or 520 R and 14.696 psi in English units; 288.71 K and 101.325 KPa in SI)
T = total

References

Arnott, R. and Small, K. 1994. The Economics of Traffic Congestion. *American Scientist* **82** (September-October): 446–455.

Ayala H., L.F. 2013. Transportation of Crude Oil, Natural Gas, and Petroleum Products. In *ASTM Handbook of Petroleum and Natural Gas Refining and Processing*, M.R. Riazi, S. Eser, J.L. Pena D., and S.S. Agrawal, Chap. 21. West Conshohocken, Pennsylvania: ASTM International.

Baker, L. 2009. Detours by Design. *Sci. Am.* **300** (2): 20–22. http://dx.doi.org/10.1038/scientificamerican0209-20.

Blumsack, S., Lave, L.B., and Ilic, M. 2007. A Quantitative Analysis of the Relationship Between Congestion and Reliability in Electric Power Networks. *Energy Journal* **28** (4): 73–100. http://dx.doi.org/10.5547/ISSN0195-6574-EJ-Vol28-No4-4.

Blumsack, S.A. 2006. *Network Topologies and Transmission Investment Under Regulation and Restructuring*. PhD dissertation, Dept. of Engineering and Public Policy, Carnegie Institute of Technology, Carnegie Mellon University, Pittsburgh, Pennsylvania (May 2006).

Braess, D. 1968. Über ein Paradoxon aus der Verkehrsplanung. *Unternehmensforschung Operations Research* **12** (1): 258–268. http://dx.doi.org/10.1007/bf01918335.

Braess, D., Nagurney, A., and Wakolbinger, T. 2005. On a Paradox of Traffic Planning. *Transportation Science* **39** (4): 446–450. http://dx.doi.org/10.1287/trsc.1050.0127.

Calvert, B. and Keady, G. 1993. Braess's paradox and power-law nonlinearities in networks. *The Journal of the Australian Mathematical Society. Series B. Applied Mathematics* **35** (1): 1–22. http://dx.doi.org/10.1017/S0334270000007256.

Calvert, B. and Keady, G. 1996. Braess's paradox and power-law nonlinearities in networks II. In *World Congress of Nonlinear Analysts, `92: Proceedings of the First, Tampa, Florida, August 19-26, 1992*, V. Lakshmanthan, Vol. III, 2223–2230. Berlin, Germany: Walter de Gruyter.

Cohen, J.E. and Horowitz, P. 1991. Paradoxical behaviour of mechanical and electrical networks. *Nature* **352** (22 August 1991): 699–701. http://dx.doi.org/10.1038/352699a0.

Energy Information Administration (EIA). 2008. About U.S. Natural Gas Pipelines—Transporting Natural Gas, http://www.eia.gov/pub/oil_gas/natural_gas/analysis_publications/ngpipeline/index.html (accessed 18 June 2012).

Fisher, M. 2002. If Northern Va. Repairs Its Roads, Traffic Will Come. *The Washington Post*, 19 October 2002.

Kolata, G. 1990. What if They Closed 42nd Street and Nobody Noticed? *The New York Times*, 25 December 1990, http://www.nytimes.com/1990/12/25/health/what-if-they-closed-42d-street-and-nobody-noticed.html.

Korilis, Y.A., Lazar, A.A., and Orda, A. 1997. Capacity allocation under noncooperative routing. *IEEE Trans. Autom. Control* **42** (3): 309–325. http://dx.doi.org/10.1109/9.557575.

Korilis, Y.A., Lazar, A.A., and Orda, A. 1999. Avoiding the Braess paradox in non-cooperative networks. *Journal of Applied Probability* **36** (1): 211–222. http://dx.doi.org/10.1239/jap/1032374242.

Kumar, S. 1987. *Gas Production Engineering*, Vol. 4. Houston, Texas: Contributions in Petroleum Geology and Engineering, Gulf Publishing Company.

Larock, B.E., Jeppson, R.W., and Watters, G.Z. 2000. *Hydraulics of Pipeline Systems*. Boca Raton, Florida: CRC Press.

Lin, W.-H. and Lo, H.K. 2009. Investigating Braess' Paradox with Time-Dependent Queues. *Transportation Science* **43** (1): 117–126 http://dx.doi.org/10.1287/trsc.1090.0258.

Menon, E. 2005. *Gas Pipeline Hydraulics*. Boca Raton, Florida: CRC Press.

Milchtaich, I. 2006. Network topology and the efficiency of equilibrium. *Games and Economic Behavior* **57** (2): 321–346. http://dx.doi.org/http://dx.doi.org/10.1016/j.geb.2005.09.005.

Mohitpour, M., Golshan, H., and Murray, A. 2007. *Pipeline Design and Construction*. New York: ASME Press.

Murchland, J. 1970. Braess' Paradox of Traffic Flow. *Transp. Res.* **4**: 391–394.

Nagurney, A. 2010. The negation of the Braess paradox as demand increases: The wisdom of crowds in transportation networks. *Europhys. Lett.* **91** (4): 48002. http://dx.doi.org/10.1209/0295-5075/91/48002.

Nagurney, A., Parkes, D., and Daniele, P. 2007. The Internet, evolutionary variational inequalities, and the time-dependent Braess paradox. *Computational Management Science* **4** (4): 355–375. http://dx.doi.org/10.1007/s10287-006-0027-7.

Osiadacz, A.J. 1987. *Simulation and Analysis of Gas Networks*. Houston, Texas: Gulf Publishing Company.

Phillips, T. 2012. *Improving natural gas network performance by quantifying the effects of Braess' Paradox*. PhD dissertation, College of Earth and Mineral Sciences, The Pennsylvania State University, University Park, Pennsylvania (May 2012).

Wolmar, C. 1994. Closure of roads seen as cure for congestion. *The Independent*, 14 October 1994, http://www.independent.co.uk/news/uk/closure-of-roads-seen-as-cure-for-congestion-1442810.html.

Appendix A—Derivation of Pipe Flow Equation for Single-Phase Flow

Total pressure losses in pipelines can be calculated as the sum of the contributions of friction losses (i.e., irreversibilities), elevation changes (potential energy differences), and acceleration changes (i.e., kinetic energy differences) as shown:

$$\left(\frac{dp}{dx}\right)_T = \left(\frac{dp}{dx}\right)_f + \left(\frac{dp}{dx}\right)_{\text{elev}} + \left(\frac{dp}{dx}\right)_{\text{acc}}. \quad \text{(A-1)}$$

Eq. A-1 is the modified Bernoulli's equation, where each of the energy terms is defined as

$$\left(\frac{dp}{dx}\right)_f = -\frac{2 f_F \rho v^2}{g_c d} \quad \text{(A-1a)}$$

$$\left(\frac{dp}{dx}\right)_{\text{elev}} = -\rho \frac{g}{g_c}\frac{dz}{dx} \quad \text{(A-1b)}$$

$$\left(\frac{dp}{dx}\right)_{\text{acc}} = -\frac{\rho v}{g_c}\frac{dv}{dx}. \quad \text{(A-1c)}$$

In pipeline flow, the contribution of the kinetic energy term to the overall energy balance is considered insignificant compared to the typical magnitudes of friction losses and potential energy changes. Thus, by integrating this expression from pipe inlet ($x=0$, $p=p_i$) to outlet ($x=L$, $p=p_j$) and considering $W=\rho v A$ with $A=\pi d^2/4$, one obtains

$$\int_{p_i}^{p_j} \rho dp = -\alpha \int_0^L dx - \beta \int_0^L \rho^2 dz, \quad \text{(A-2)}$$

where $\alpha = (32 W^2 f)/(\pi^2 g_c d^5)$, $\beta = (g/g_c)(\Delta h/L)$.

For the flow of liquids and nearly incompressible fluids, density integrals can be readily resolved and volumetric flow through a horizontal pipe is shown to be dependent on the difference of linear end pressures ($s=1$), corresponding to the Darcy-Weisbach equation ($q_{ij} = C_{ij} \cdot \sqrt{p_i - p_j}$) in Table 1. The use of Poiseuille's law for laminar flow in the evaluation of friction factors for liquid flow further establishes a linear dependency between pressure drop and flow rate [$q_{ij} = C_{ij} \cdot (p_i - p_j)$] shown in Table 1. For the isothermal flow of gases, the fluid density dependency with pressure ($\rho = \eta p$, where $\eta = SG_G MW_{\text{air}}/RT_{\text{av}}Z_{\text{av}}$) introduces a stronger dependency of flow rate on pressure and yields for horizontal pipes ($\beta=0$:)

$$q_{ij} = C_{ij} \cdot \sqrt{p_i^2 - p_j^2}, \quad \text{(A-3)}$$

where gas flow has been evaluated at standard conditions, $W = \rho_{sc} q_{Gsc}$ with $\rho_{sc} = (p_{sc}\gamma_g MW_{\text{air}})/(R \cdot T_{sc})$. Eq. A-3 states the well-known fact that the driving force for gas flow through pipelines is the difference of the squared pressures ($s=2$). In this equation, C_{ij} is the pipe conductivity to gases given by

$$C_{ij} = \left(\frac{\pi^2 g_c R}{64 MW_{\text{air}}}\right)^{0.5} \frac{T_{sc}/p_{sc}}{(SG_G T_{av} Z_{av})^{0.5}} \frac{d^{2.5}}{f_F^{0.5} L^{0.5}},$$

and which captures the dependency of friction factor, pipe geometry, and fluid properties on the flow capacity of the pipe. Depending on the type of friction factor correlation used to evaluate pipe conductivity, Eq. A-3 can be recast into the different traditional forms of gas-pipe-flow equations available in the literature such as the equations of Weymouth, Panhandle-A, Panhandle-B, and AGA shown in Table 1 and other popular forms (Ayala 2012; Mohitpour et al. 2007; Menon 2005; Kumar 1987; Osiadacz 1987).

Appendix B—Unconstrained Wheatstone Structures

In terms of its linear analog, the pressure response of the unconstrained Wheatstone network structure delivering a total and fixed rate Q_t of natural gas at a fixed delivery pressure specification at node 4 (p_4) is given by

$$\begin{bmatrix} -(L_{12}+L_{13}) & L_{12} & L_{13} \\ L_{12} & -(L_{12}+L_{24}+L_{23}) & L_{23} \\ L_{13} & L_{23} & -(L_{34}+L_{13}+L_{23}) \end{bmatrix} \begin{bmatrix} p_1 \\ p_2 \\ p_3 \end{bmatrix} = \begin{bmatrix} -Q_t \\ -L_{24}p_4 \\ -L_{34}p_4 \end{bmatrix}, \quad \text{(B-1)}$$

From where it follows

$$(p_1 - p_4) = \frac{\Omega_a + L_{23} \cdot \Omega_b}{\Omega_c + L_{23} \cdot \Omega_d} \cdot Q_t, \quad \text{(B-2)}$$

where

$$\Omega_a = L_{12}L_{34} + L_{24}L_{13} + L_{12}L_{13} + L_{34}L_{24},$$

$$\Omega_b = L_{12}L_{34} + L_{24}L_{13\text{w}}, \; \Omega_c = L_{12}L_{34}L_{24} + L_{34}L_{24}L_{13} + L_{12}L_{34}L_{13} + L_{12}L_{24}L_{13},$$

and $\Omega_d = L_{12}L_{34} + L_{34}L_{13} + L_{12}L_{24} + L_{24}L_{13}$.

If the behavior of $\partial(p_1 - p_4)/\partial L_{23}$ is now explored, one obtains

$$\frac{\partial(p_1 - p_4)}{\partial L_{23}} = Q_t \cdot \frac{\Omega_b \cdot (\Omega_c + L_{23} \cdot \Omega_d) - \Omega_d \cdot (\Omega_a + L_{23} \cdot \Omega_b)}{(\Omega_c + L_{23} \cdot \Omega_d)^2}. \quad \text{(B-3)}$$

According to Eq. B-3, paradoxical behavior [$\partial(p_1 - p_4)/\partial L_{23} > 0$] can only occur in this system if

$$\Omega_b \cdot \Omega_c - \Omega_a \cdot \Omega_d > 0, \quad \text{(B-4)}$$

which collapses the following expression:

$$(L_{12} \cdot L_{34} - L_{24} \cdot L_{13})^2 < 0 \quad \text{(B-5)}$$

once the Ω's definitions are substituted. The expression in Eq. B-5 is never negative regardless of conductivity values.

Appendix C—Embedded Wheatstone Structures

The pressure response of an unconstrained Wheatstone network transporting a known total rate Q_t to nodes 2 and 4, where a k^*Q_t fraction ($0<k<1$) is demanded at node 2 and the rest is delivered at node 4, can be written in terms of its linear analog as follows:

$$\begin{bmatrix} -(L_{12}+L_{13}) & L_{12} & L_{13} \\ L_{12} & -(L_{12}+L_{24}+L_{23}) & L_{23} \\ L_{13} & L_{23} & -(L_{34}+L_{13}+L_{23}) \end{bmatrix} \begin{bmatrix} p_1 \\ p_2 \\ p_3 \end{bmatrix} = \begin{bmatrix} -Q_t \\ -L_{24}p_4 + kQ_t \\ -L_{34}p_4 \end{bmatrix}, \quad \text{(C-1)}$$

where the pressure at node 4 is assumed to be known or specified. The solution of this system of equations yields:

$$(p_1 - p_4) = \frac{\Omega_a - k \cdot \Omega_e + L_{23} \cdot (\Omega_b - k \cdot \Omega_f)}{\Omega_c + L_{23} \cdot \Omega_d} \cdot Q_t, \quad \text{(C-2)}$$

where $\Omega_a, \Omega_b, \Omega_c, \Omega_d$ have been defined previously (Appendix B), $\Omega_e = L_{12} \cdot (L_{34} + L_{13})$, and $\Omega_f = L_{13} + L_{12}$. By differentiating Eq. C-2, it can be demonstrated that a change in sign for $\partial(p_1 - p_4)/\partial L_{23}$ occurs in this system at the following critical value of the k-fluid takeoff fraction:

$$k_c = \frac{L_{12}L_{34} - L_{24}L_{13}}{L_{34}(L_{12} + L_{13})} \quad \text{(C-3)}$$

for the linear analog model. A value of $k>k_c$ implies $\partial(p_1 - p_4)/\partial L_{23}>0$, and thus the existence of the Braess paradox for the linear system.

Luis F. Ayala H. is Associate Professor of Petroleum and Natural Gas Engineering and Associate Department Head for Graduate Education in the John and Willie Leone Family Department of Energy and Mineral Engineering at Pennsylvania State University. email: ayala@psu.edu. His research activities focus on the areas of natural gas engineering, hydrocarbon phase behavior, and numerical modeling. He holds two engineering degrees in chemical engineering and another in petroleum engineering from Universidad de Oriente, Venezuela, and MS and PhD degrees in petroleum and natural gas engineering from Pennsylvania State University. He was awarded the 2007 Outstanding Technical Editor Award by SPE and has served as the Editor-in-Chief of *The Way Ahead,* the SPE flagship magazine designed by and for young professionals in oil and gas, and is currently an Associate Editor for the *SPE Reservoir Evaluation and Engineering* Journal and a member of the SPE Reservoir Description and Dynamics Advisory Committee.

Seth Blumsack is Assistant Professor of Energy Policy and Economics in the John and Willie Leone Family Department of Energy and Mineral Engineering at Pennsylvania State University. email: blumsack@psu.edu. His research interests include the intersection of engineering, economics, and the regulation of energy and electric power systems. He is currently the John T. Ryan Jr. Faculty Fellow in the College of Earth and Mineral Sciences at Penn State and an Adjunct Research Professor with the Carnegie Mellon Electricity Industry Center. He holds a BA degree in mathematics and economics from Reed College, and MS and PhD degrees in economics and engineering and public policy, respectively, both from Carnegie-Mellon University.